

Equilibrium positions of the elasto-inertial particle migration in rectangular channel flow of Oldroyd-B viscoelastic fluids

Zhaosheng Yu^{1,†}, Peng Wang¹, Jianzhong Lin^{1,†} and Howard H. Hu²

¹State Key Laboratory of Fluid Power and Mechatronic Systems, Department of Mechanics, Zhejiang University, Hangzhou 310027, PR China

²Department of Mechanical Engineering and Applied Mechanics, University of Pennsylvania, Philadelphia, PA 19104-6315, USA

(Received 22 February 2018; revised 26 February 2019; accepted 28 February 2019;
first published online 11 April 2019)

In this paper, the lateral migration of a neutrally buoyant spherical particle in the pressure-driven rectangular channel flow of an Oldroyd-B fluid is numerically investigated with a fictitious domain method. The aspect ratio of the channel cross-section considered is 1 and 2, respectively. The particle lateral motion trajectories are shown for the bulk Reynolds number ranging from 1 to 100, the ratio of the solvent viscosity to the total viscosity being 0.5, and a Weissenberg number up to 1.5. Our results indicate that the lateral equilibrium positions located on the cross-section midline, diagonal line, corner and channel centreline occur successively as the fluid elasticity is increased, for particle migration in square channel flow with finite fluid inertia. The transition of the equilibrium position depends strongly on the elasticity number (the ratio of the Weissenberg number to the Reynolds number) and weakly on the Reynolds number. The diagonal-line equilibrium position occurs at an elasticity number ranging from roughly 0.001 to 0.02, and can coexist with the midline and corner equilibrium positions. When the fluid inertia is negligibly small, particles migrate towards the channel centreline, or the closest corner, depending on their initial positions and the Weissenberg number, and the corner attractive area first increases and then decreases as the Weissenberg number increases. For particle migration in a rectangular channel with an aspect ratio of 2, the transition of the equilibrium position from the midline, ‘diagonal line’ (the line where two lateral shear rates are equal to each other), off-centre long midline and channel centreline takes place as the Weissenberg number increases at moderate Reynolds numbers. An off-centre equilibrium position on the long midline is observed for a large blockage ratio of 0.3 (i.e. the ratio of the particle diameter to the channel height is 0.3) at a low Reynolds number. This off-centre migration is driven by shear forces, unlike the elasticity-induced rapid inward migration, which is driven by the normal force (pressure or first normal stress difference).

Key words: microfluidics, particle/fluid flow, viscoelasticity

† Email addresses for correspondence: yuzhaosheng@zju.edu.cn, jzlin@zju.edu.cn

1. Introduction

The lateral migration of particles in pipe or channel flows has been a classic and important problem in the field of fluid mechanics since Segre & Silberberg (1961) observed that spherical particles moved into a thin annular region located at roughly 0.6 tube radius away from the tube axis in tube flow. The perturbation analyses revealed that the inertia-induced lift force is responsible for the particle migration in Newtonian shear flows (Ho & Leal 1974; Matas, Morris & Guazzelli 2009). Matas, Morris & Guazzelli (2004) extended the Segre–Silberberg experiments to moderately high Reynolds numbers up to 2400. They observed that the Segre–Silberberg particle annulus equilibrium radial position moved towards the wall as the Reynolds number (Re) was increased, and an additional inner annulus appeared at Re larger than around 600. The numerical results of Shao, Yu & Sun (2008) confirmed the presence of the inner particle equilibrium position, which shifted closer to the tube axis with increasing Reynolds number, in association with the particle-induced flow structure in pipe flow at moderately high Reynolds numbers. On the other hand, Karnis & Mason (1966) observed that the particle migrated towards the tube axis in a viscoelastic fluid. Both three-dimensional numerical simulations and microfluidic experiments of D’Avino *et al.* (2012) demonstrated the presence of a bistability scenario for the migration of particles suspended in a viscoelastic liquid flowing in a pipe: particles migrated either towards the centreline or to the wall, depending on the rheological properties of the suspending liquid and the relative dimensions of the particle and tube. They also provided simple design rules for particle viscoelastic focusing under flow in micro-pipes.

The inertial and viscoelastic migration of particles has attracted substantial attention in the microfluidic community since the pioneering works of Di Carlo *et al.* (2007) and Leshansky *et al.* (2007), who implemented particle inertial and viscoelastic migration, respectively, in microchannels for particle separation. This particle separation technology is promising due to its advantages of simple, continuous and high-throughput manipulation. Straight square- or rectangular-shaped microchannels have been widely used for inertial and viscoelastic focusing, but the fundamentals of particle migration in square or rectangular channel flows are not yet fully understood, particularly for the viscoelastic case. In the following, we first summarize work on the particle inertial migration in square or rectangular channel flows of Newtonian fluids.

Regarding the square channel, the experiments of Choi, Seo & Lee (2011) at relatively low Reynolds numbers indicated that the particles first migrated rapidly towards the channel walls along the cross-stream direction and then migrated slowly to the face centres. The numerical results of Chun & Ladd (2006) showed that there existed eight lateral particle equilibrium positions at $Re = 100$ (based on the channel width and average velocity), including four face centres and four channel corners, and the face-centre equilibrium positions became unstable as the Reynolds number increased. Abbas *et al.* (2014) investigated experimentally and numerically the particle lateral migration in square channels for Re up to 120, and their numerical results for $Re = 120$ showed that the particles migrated to the face centre in a long computational domain, whereas they migrated to the corner in a very short computational domain, thus providing an explanation for the stable corner equilibrium position at $Re = 100$ of Chun & Ladd (2006), who employed a relatively short channel for the determination of the equilibrium positions of one particle. Kazuma, Tomoaki & Masako (2014) examined experimentally the inertial migration of neutrally buoyant spherical particles in square channel flows in the range of Reynolds numbers from 100 to 1200, and

observed that the particles migrated to eight equilibrium positions located at the centres of the channel faces and the channel corners at high Reynolds numbers. For a rectangular duct with an aspect ratio not being unity, Zhou & Papautsky (2013) claimed that the particles migrate rapidly towards the longer channel sidewalls at the first stage and then migrate slowly to the face centres of the longer sidewalls at the second stage. Liu *et al.* (2015a) observed additional stable equilibrium positions at the face centres of the shorter walls when the Reynolds number exceeded a critical value, which depended on the aspect ratio of the channel cross-section and the particle size.

In rectangular- or square-shaped channels, the fluid viscoelasticity, coupled with fluid inertia and wall confinement effects, leads to more complex dynamics of the particle migration. Leshansky *et al.* (2007) conducted an experiment on the particle migration in viscoelastic fluids in a rectangular micro-slit with a large aspect ratio, and observed that particles migrated towards the channel midplane parallel to the longer walls at low Reynolds numbers. Villone *et al.* (2011) investigated numerically the effects of fluid rheological properties on the particle migration in a micro-slit by adopting the Giesekus model and the Phan-Thien–Tanner (PTT) model. Their results showed that, for small confinement ratios (i.e. particle/channel size ratio), the particle migrated towards the channel centre-plane or the closest wall, depending on its initial position. For large confinement ratios, the particle migrated towards the wall in a PTT fluid, whereas the particle migrated towards the centre-plane in a Giesekus fluid with a comparable amount of shear thinning. For the square channel flow without inertial effects, the numerical results of Villone *et al.* (2013) showed that the particle in a PTT fluid migrated towards the channel centreline or the closest corner depending on its initial position, and the centre attractive region was reduced as the fluid viscoelasticity was increased. For a Giesekus fluid, the secondary flow could trap some particles in the vortex structure, and as the particle size was increased or the Deborah number was reduced, the cross-streamline migration velocity overcame the secondary flow velocity and most of the particles were driven towards the channel centreline. Multiple equilibrium positions (channel centreline and corners) were experimentally observed for rigid colloidal particles in a square channel, whereas a single array along the centreline of the channel was observed for flexible DNA molecules (Kim *et al.* 2012) and red blood cells (Yang *et al.* 2012) presumably due to the flexibility-induced wall lift force.

The fluid inertial effect was found to be beneficial to the particle focusing on the channel centreline in a viscoelastic fluid – so-called elasto-inertial particle focusing (Lim *et al.* 2014; Seo, Kang & Lee 2014; Kim & Kim 2016). Lim *et al.* (2014) observed particle migration towards the channel centreline in weakly elastic fluids ($El \sim 0.1$, El being the elasticity number, i.e. the ratio of the Weissenberg number to the Reynolds number) over a wide range of Reynolds numbers $10 \leq Re \leq 10^4$. The viscoelastic force normally drives the particles towards the channel centreline or the corners, and it was assumed by Yang *et al.* (2011) and Seo *et al.* (2014) that the fluid inertia provides a wall repulsive force (or lift force) which pushes the particles out of the corners. Li, McKinley & Ardekani (2015) simulated the elasto-inertial particle migration in the midplane of a square channel with the Oldroyd-B and Giesekus viscoelastic models. Their results indicated that the equilibrium position depended on the interplay between the elastic and inertial effects, and particle focusing at the centreline occurred in flows with strong elasticity and weak inertia for the Oldroyd-B fluid. Both shear-thinning effects and secondary flows tended to move the particle away from the channel centreline, and the effect was more pronounced as

inertia and elasticity effects increased. Raffiee, Dabiri & Ardekani (2017) investigated numerically both inertial and elasto-inertial migration of a deformable capsule in a square channel. They observed that the equilibrium position of the capsule was on the channel diagonal line, in contrast to that of a rigid particle, which was on the centre of the channel faces for the same range of Reynolds number in a Newtonian fluid, and the constant-viscosity viscoelastic fluid (an Oldroyd-B fluid) tended to push the cells towards the centreline. Trofa *et al.* (2015) investigated the elasto-inertial particle migration in a two-dimensional Poiseuille flow with a finite-element method, and observed that, for comparable values of the Deborah and Reynolds numbers, the migration was dominated by fluid elasticity and that at moderately high Reynolds numbers the regime transition occurred through two bifurcations.

There are few fundamental works on the elasto-inertial particle migration in a rectangular channel with a moderate aspect ratio $AR = 2-4$. The experimental results of Liu *et al.* (2015*b*) demonstrated that large particles (particle/channel size ratio being 0.3) migrated towards the lateral positions near the shorter sidewalls, whereas smaller particles migrated towards the channel centreline. Xiang, Dai & Ni (2016) observed in their experiments that the particles migrated towards two off-centre positions in the planes parallel to the shorter walls, and with further increasing flow rate, a third focusing position occurred at the channel centre. Di, Lu & Xuan (2016) observed off-centre particle focusing positions for a rectangular channel with the aspect ratio of 2 filled with polyethylene oxide (PEO) fluid at low Reynolds numbers. Recently, Wang, Yu & Lin (2018) investigated numerically the lateral migration of a neutrally buoyant spherical particle in a rectangular channel flow of Giesekus viscoelastic fluids with a fictitious domain method. It was shown that, when both fluid inertial and elastic effects were important, most particles migrated towards the face centres of the shorter walls and the particle migration trajectories were significantly affected by the secondary flow. We note that nice reviews on the particle migration in viscoelastic liquids were presented by D'Avino & Maffettone (2015), D'Avino, Greco & Maffettone (2017), Lu *et al.* (2017) and Yuan *et al.* (2018).

In the present study, we aim to investigate the elasto-inertial particle migration in rectangular (including square) channel flow of an Oldroyd-B viscoelastic fluid by means of three-dimensional direct numerical simulations. We are concerned with the particle migration behaviour in the entire channel. Owing to the drawback of our code being incapable of dealing with relatively high Weissenberg numbers and the difficulty in exactly modeling the rheological properties of the actual fluids in the experiments, we do not intend to reproduce or unambiguously explain the experimental results mentioned earlier. In the experiments of Liu *et al.* (2015*b*) and Xiang *et al.* (2016), the typical Reynolds number was in the range of 0.1–10, and the elasticity number was much larger than unity. Nevertheless, we have managed to reproduce some experimental observations in a qualitative sense. The primary merits of the present study are that an equilibrium position located on the line in the channel cross-section where the shear rates in two lateral directions are the same (i.e. the diagonal line for the square duct) is revealed for the elasto-inertial migration of a rigid spherical particle in rectangular channel flow at low elasticity numbers, and that an off-centre elasticity-induced equilibrium position on the long midline of a rectangular channel is reproduced numerically for a large particle at low Reynolds numbers.

The rest of paper is organized as follows. The numerical method is outlined and validated in § 2. In § 3, the results on the particle migration trajectories in a square channel and a rectangular channel with an aspect ratio of 2 at different Reynolds and Weissenberg numbers are presented and discussed successively. The concluding remarks are given in § 4.

2. Numerical model

2.1. Fictitious domain method

The direct forcing/fictitious domain (DF/FD) method proposed by Yu & Shao (2007) is employed here to simulate the particle motion in a rectangular channel. This method is an improved version of the earlier distributed Lagrange multiplier/fictitious domain (DLM/FD) code (Yu *et al.* 2002; Yu, Wachs & Peysson 2006; Yu & Wachs 2007). The DLM/FD method was originally developed by Glowinski *et al.* (1999). The main idea of this method is that the interior of the particle is filled with the fluid and a pseudo body force (i.e. distributed Lagrange multiplier) is introduced over the particle inner domain to force the fictitious fluid to satisfy the rigid-body motion constraint. We only briefly describe the algorithm of the DF/FD method in the following; the reader is referred to Yu & Shao (2007) for further details of the method.

For simplicity of description, we consider only one particle in the following formulae. Suppose that the particle density, volume, moment of inertia, translational velocity and angular velocity are ρ_s , V_p , J , \mathbf{U} and $\boldsymbol{\omega}_p$, respectively. The fluid solvent viscosity and polymer viscosity are η_s and η_p , respectively. The fluid density is ρ_f . Let $P(t)$ represent the solid domain and Ω the entire domain including the interior and exterior of the solid body. We introduce the following scales for the non-dimensionalization: H for length, U_0 for velocity, H/U_0 for time, $\rho_f U_0^2$ for pressure and $\rho_f U_0^2/H$ for the pseudo body force. Thus, the dimensionless FD formulation for an incompressible fluid comprises the following three parts:

(1) Combined momentum equations

$$\frac{\partial \mathbf{u}}{\partial t} + \mathbf{u} \cdot \nabla \mathbf{u} = \frac{\eta_r \nabla^2 \mathbf{u}}{Re} - \nabla p + \frac{(1 - \eta_r) \nabla \cdot \mathbf{B}}{Re Wi} + \boldsymbol{\lambda} \quad \text{in } \Omega, \quad (2.1)$$

$$\mathbf{u} = \mathbf{U} + \boldsymbol{\omega}_p \times \mathbf{r} \quad \text{in } P(t), \quad (2.2)$$

$$(\rho_r - 1) V_p^* \frac{d\mathbf{U}}{dt} = - \int_P \boldsymbol{\lambda} d\mathbf{x}, \quad (2.3)$$

$$(\rho_r - 1) J^* \frac{d\boldsymbol{\omega}_p}{dt} = - \int_P \mathbf{r} \times \boldsymbol{\lambda} d\mathbf{x}. \quad (2.4)$$

(2) Continuity equation

$$\nabla \cdot \mathbf{u} = 0 \quad \text{in } \Omega. \quad (2.5)$$

(3) Oldroyd-B constitutive equation

$$\frac{\partial \mathbf{B}}{\partial t} + \mathbf{u} \cdot \nabla \mathbf{B} - \mathbf{B} \cdot \nabla \mathbf{u} - (\nabla \mathbf{u})^T \cdot \mathbf{B} + \frac{\mathbf{B} - \mathbf{I}}{Wi} = 0 \quad \text{in } \Omega. \quad (2.6)$$

In the above equations, \mathbf{u} represents the fluid velocity, p the fluid pressure, $\boldsymbol{\lambda}$ the Lagrange multiplier that is defined in the solid domain $P(t)$, \mathbf{r} the position vector with respect to the centre of mass of the particle, ρ_r the particle/fluid density ratio defined by $\rho_r = \rho_s/\rho_f$, Re the Reynolds number defined by $Re = \rho_f U_0 H/\eta_0$ (η_0 being the total zero-shear-rate viscosity of the fluid $\eta_0 = \eta_s + \eta_p$), V_p^* the dimensionless particle volume defined by $V_p^* = V_p/H^3$, J^* the dimensionless moment of inertia defined by $J^* = J/\rho_s H^5$, η_r the ratio of the solvent viscosity (η_s) to the total zero-shear-rate viscosity of the fluid (η_0), Wi the Weissenberg number defined as $Wi = \lambda_t U_0/H$

(λ_t being the fluid relaxation time), and \mathbf{B} the polymer configuration tensor which is related to the polymer stress tensor $\boldsymbol{\tau}$ via $\boldsymbol{\tau} = \eta_p(\mathbf{B} - \mathbf{I})/\lambda_t$.

A fractional-step time scheme is used to decouple systems (2.1)–(2.6) into the following three subproblems.

- (1) Fluid subproblem for \mathbf{u}_f^* and p :

$$\frac{\mathbf{u}^* - \mathbf{u}^n}{\Delta t} - \frac{\eta_r \nabla^2 \mathbf{u}^*}{2Re} = -\nabla p + \frac{1}{2}[3G^n - G^{n-1}] + \frac{\eta_r \nabla^2 \mathbf{u}^n}{2Re} + \boldsymbol{\lambda}^n, \quad (2.7)$$

$$\nabla \cdot \mathbf{u}^* = 0, \quad (2.8)$$

where $G = -\mathbf{u} \cdot \nabla \mathbf{u} + [(1 - \eta_r)/ReWi]\nabla \cdot \mathbf{B}$. This subproblem is essentially the solution of the Navier–Stokes equation. An efficient finite-difference-based projection method on a homogeneous half-staggered grid is employed Yu & Shao (2007). All spatial derivatives are discretized with the second-order central difference scheme.

- (2) Particle subproblem for \mathbf{U}^{n+1} , $\boldsymbol{\omega}_p^{n+1}$, $\boldsymbol{\lambda}^{n+1}$, \mathbf{u}^{n+1} :

$$\rho_r V_p^* \frac{\mathbf{U}^{n+1}}{\Delta t} = (\rho_r - 1) V_p^* \frac{\mathbf{U}^n}{\Delta t} + \int_p \left(\frac{\mathbf{u}^*}{\Delta t} - \boldsymbol{\lambda}^n \right) \mathbf{d}\mathbf{x}, \quad (2.9)$$

$$\rho_r \frac{\mathbf{J}^* \boldsymbol{\omega}_p^{n+1}}{\Delta t} = (\rho_r - 1) \frac{\mathbf{J}^* \boldsymbol{\omega}_p^n}{\Delta t} + \int_p \mathbf{r} \times \left(\frac{\mathbf{u}^*}{\Delta t} - \boldsymbol{\lambda}^n \right) \mathbf{d}\mathbf{x}. \quad (2.10)$$

Note that the above equations have been reformulated so that all the terms on the right-hand side are known quantities and consequently the particle velocities \mathbf{U}^{n+1} and $\boldsymbol{\omega}_p^{n+1}$ are obtained without iteration. Then, the Lagrange multipliers defined at the Lagrangian nodes are determined from

$$\boldsymbol{\lambda}^{n+1} = \frac{\mathbf{U}^{n+1} + \boldsymbol{\omega}_p^{n+1} \times \mathbf{r} - \mathbf{u}^*}{\Delta t} + \boldsymbol{\lambda}^n. \quad (2.11)$$

Finally, the fluid velocities \mathbf{u}^{n+1} at the Eulerian nodes are corrected from

$$\mathbf{u}^{n+1} = \mathbf{u}^* + \Delta t(\boldsymbol{\lambda}^{n+1} - \boldsymbol{\lambda}^n). \quad (2.12)$$

In the above manipulations, the tri-linear function is used to transfer the fluid velocity from the Eulerian nodes to the Lagrangian nodes, and distribute the pseudo body force from the Lagrangian nodes to the Eulerian nodes. For the spherical particle studied, the Lagrangian nodes are distributed on a sequence of spherical surface (Yu & Shao 2007).

- (3) Constitutive equation subproblem for \mathbf{B}

$$\frac{\mathbf{B}^{n+1} - \mathbf{B}^n}{\Delta t} + \mathbf{u}^{n+1} \cdot \nabla \mathbf{B}^n - \mathbf{B}^n \cdot \nabla \mathbf{u}^{n+1} - (\nabla \mathbf{u}^{n+1})^T \cdot \mathbf{B}^n + \frac{\mathbf{B}^{n+1} - \mathbf{I}}{Wi} = 0. \quad (2.13)$$

In the above equation \mathbf{u}^{n+1} has been obtained from the first two subproblems. For simplicity, only the first-order time scheme is used for the constitutive equation. For the spatial schemes, the convective term is discretized with a third-order upwinding MUSCL scheme (van Leer 1979) and the velocity gradient is discretized with the central difference scheme.

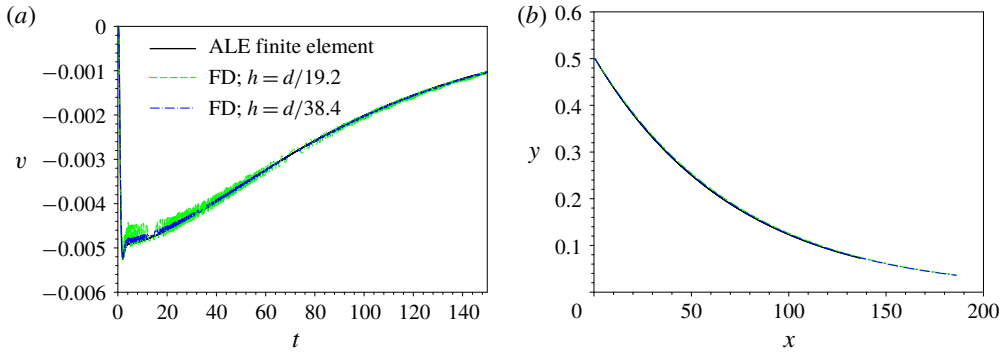


FIGURE 1. (Colour online) (a) Time development of the lateral velocity and (b) the trajectory of the particle in a two-dimensional Poiseuille flow of Oldroyd-B fluids obtained from our fictitious domain method and the ALE finite element method of Hu *et al.* (2001). Here $Re = \rho_f U_0 H / (2\eta_0) = 1.0$, $Wi = 2\lambda_t U_0 / H = 0.5$ and $d/H = 0.15$.

Our fictitious domain method has been widely used and verified in previous work (Yu *et al.* 2002, 2006; Yu & Shao 2007; Yu & Wachs 2007; Shao *et al.* 2008). Here, we further validate our FD method by comparing the numerical results on particle migration in a two-dimensional Poiseuille flow of Oldroyd-B fluids to those obtained from the ALE finite element code of Hu, Patankar & Zhu (2001). The length and the time are scaled as the half channel height $H/2$ and the maximum velocity at the channel centre U_0 , respectively. The parameters are $Re = \rho_f U_0 H / (2\eta_0) = 1.0$, $Wi = 2\lambda_t U_0 / H = 0.5$ and $\eta_r = \eta_s / \eta_0 = 0.5$. The ratio of the particle diameter to the channel height is $d/H = 0.15$. The computational domain size is $2H \times H$, with the dimensionless values of 4×2 , and the y -coordinate ranging from -1 to 1 . The particle is released at $y_0 = 0.5$. For the fictitious domain method, two grid sizes $h = H/128$ (i.e. $h = d/19.2$, d being particle diameter) and $h = H/256$ (i.e. $h = d/38.4$) are used, respectively, and the time step $\Delta t = 5 \times 10^{-4}$ is employed. For the ALE code, there are 36 segments on the particle surface and in total 21 723 nodes for the mesh, and the time step is 0.005. The ALE results have been found to be perfectly independent of the mesh and time resolutions. The time development of the lateral velocity and the trajectory of the particle obtained from the two methods are compared in figure 1(a) and 1(b), respectively. It can be seen that our FD results are in good agreement with the ALE results, particularly on the particle trajectory. From figure 1(a), the FD result from $h = d/38.4$ is more accurate and smooth compared to that from $h = d/19.2$. Nevertheless, we choose typically $h = d/19.2$ for the following three-dimensional computations, due to the use of the homogeneous mesh and our limited computational resources. The ALE method is better suited to the present problem where only one particle is involved; however, the ALE code of Hu *et al.* (2001) is currently incapable of dealing with the three-dimensional pressure-driven flow because it cannot generate the periodic mesh in three dimensions.

2.2. Simulation set-up

In the present study, we are concerned with the lateral motion of a solid neutrally buoyant particle in a straight rectangular channel filled with an Oldroyd-B viscoelastic fluid. A Cartesian reference frame is considered with its origin at the channel centre. The schematic diagram of the channel is shown in figure 2. The periodic boundary

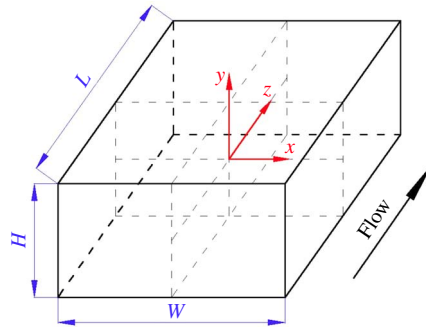


FIGURE 2. (Colour online) Schematic diagram of the rectangular channel flow.

condition is imposed in the streamwise direction and a constant pressure gradient is introduced to sustain the channel flow. The channel height, width and length (period) are denoted by H , W and L , respectively. The computational domain spans over $[-W/2, W/2]$, $[-H/2, H/2]$ and $[-L/2, L/2]$ in the x , y and z directions, respectively. The characteristic length is the channel height H , and the characteristic velocity is the maximum velocity at the channel centreline U_0 under a given pressure gradient. The latter is $U_0 = 16\kappa(-dp/dx)H^2/\eta_0\pi^3$, where κ is a constant depending on the geometry of the channel ($\kappa \approx 0.143$ for a square channel and $\kappa \approx 0.221$ for a rectangular channel with the aspect ratio of 2, filled with the Newtonian or Oldroyd-B fluid). The Reynolds and Weissenberg numbers (Re and Wi) are based on the maximum velocity U_0 and the channel height, i.e. $Re = \rho_f U_0 H / \eta_0$ and $Wi = \lambda_i U_0 / H$. The ratio of Wi to Re is defined as the elasticity number, $El = Wi / Re = \lambda_i \eta_0 / \rho_f H^2$, which depends only on the channel dimension and fluid properties. The ratio d/H of the particle diameter d to the channel height H is defined as the blockage ratio; typically, $d/H = 0.15$. Throughout this study, $\eta_r = 0.5$. The mesh size is $h = H/128$, corresponding to 19.2 grid points across the particle diameter for $d/H = 0.15$, and the time step is $\Delta t = 5 \times 10^{-4}$. Because we adopt a homogeneous grid, a relatively short channel is chosen, $L = H$, in order to save on computational cost. For the case of a typical rectangular channel with the mesh number being $256 \times 128 \times 128$, it took around one month to run 600 time units (i.e. 1.2 million time loops). The distance between the particles in two neighbouring periodic cells is around 6.7 particle diameters for $d/H = 0.15$. Our test presented later shows that this channel length is not sufficiently large to eliminate the hydrodynamic interactions between neighbouring particles, but the effect is not so significant to produce qualitatively different results (see figure 9). In practical particle focusing or separation applications, many particles are involved and particle hydrodynamic interactions normally exist.

3. Results and discussion

In this section, the particle lateral migration induced by fluid viscoelasticity and inertia is examined through particle trajectories. We mainly investigated the effects of the Reynolds, Weissenberg and elasticity numbers in the range of $Re = 1-100$, $Wi = 0.01-1.5$ and $El = 0.0002-1.0$. The simulations are performed by considering the entire channel as the computational domain. However, due to geometric symmetry, the particle trajectories are presented only in the upper-right quadrant of the cross-section of the rectangular channel (and a half-quadrant for the square channel, delimited

by the midline and diagonal lines). In all trajectory figures below, the dash-dotted lines represent the position where particles touch the wall, the big dots denote the particle initial positions, and the small dots represent the particle positions on the particle trajectories when the particles travel every 100 dimensionless time units. We first examine the results on the particle migration for the square channel flow at a low Reynolds number $Re = 1$, where the fluid inertia is expected to be insignificant, and at moderate Reynolds numbers $Re = 10, 50$ and 100 , where the fluid inertia is significant. A phase diagram for the equilibrium positions with respect to the Reynolds and elasticity numbers is presented. We then report the results on the particle migration in a rectangular channel with an aspect ratio of 2, in order to show that a similar ‘diagonal-line’ equilibrium position located on the line where the shear rates in two lateral directions are the same also exists for the non-square rectangular channel.

3.1. Particle migration in square channel flow

3.1.1. Viscoelasticity-induced migration at a low Reynolds number $Re = 1$

We now examine the particle migration in square channel flow at a low Reynolds number $Re = 1$. Note that the particle Reynolds number based on the particle size and the shear rate is around $(d/H)^2 Re = 0.0225$. Therefore, the fluid inertial effect on the particle motion is expected to be small. Initially, both the particle and fluid are at rest. Figure 3 shows the trajectories of particles released at different positions projected in the channel cross-section for $Re = 1$, $d/H = 0.15$ and different Weissenberg numbers $Wi = 0.01, 0.1, 0.5$ and 1.0 (the elasticity number being $0.01, 0.1, 0.5$ and 1.0 , respectively). For $Wi = 0.01$, almost all particles migrate towards the channel centreline, except those released in a very small corner region (figure 3a). For $Wi = 0.1$, the particles released near the wall move towards the corner along the wall, and the other particles migrate towards the channel centreline (figure 3b). As Wi increases from 0.01 to 0.5 , the corner attractive region is enlarged, and as Wi further increases to 1.0 , the corner attractive region begins to shrink, as shown in figure 3 where the corner attractive region is marked by the red closed lines. From our results, most particles initially distributed homogeneously in a square channel filled with a viscoelastic fluid with constant viscosity even at high Weissenberg numbers and low Reynolds numbers would migrate to the channel centre region, consistent with previous experimental observations (Del Giudice *et al.* 2015; Liu *et al.* 2015b). It has been recognized that the shear-thinning effect of the viscoelastic fluid tends to make the particles move towards the wall or the corner (Villone *et al.* 2013; Del Giudice *et al.* 2015; Liu *et al.* 2015b). From figure 3, the particle migration rate is overall increased with increasing Weissenberg number.

In addition, figure 3 shows that the particles released near the corner attractive region first migrate towards the diagonal line and then move towards the channel centreline along the diagonal line. Particles migrate towards the channel centreline normally along curved lines particularly for $Wi \geq 0.1$ as if they were attracted by the diagonal line, except for the particles released directly on the midline or the diagonal line, which migrate along a straight line due to symmetry confinement.

3.1.2. Elasto-inertial migration at $Re = 10, Re = 50$ and $Re = 100$

Figure 4 shows the particle trajectories projected in the channel cross-section at $Re = 10$, and $Wi = 0.01, 0.05, 0.1$ and 0.5 (the elasticity number being $0.001, 0.005, 0.01$ and 0.05 , respectively). For $Wi = 0.01$ ($El = 0.001$), the elasticity effect is

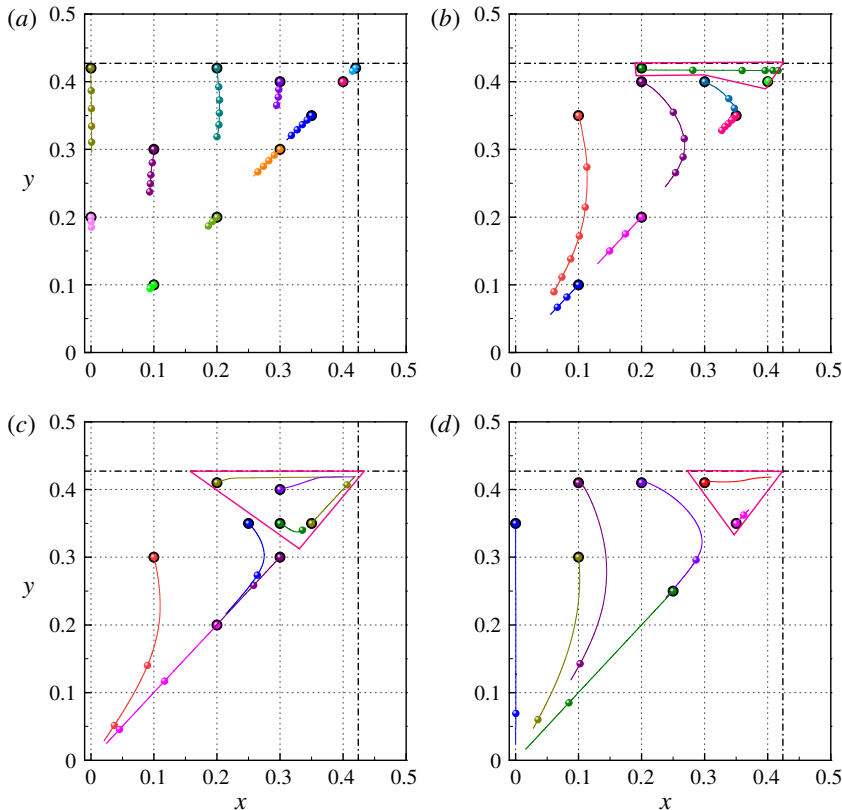


FIGURE 3. (Colour online) Particle trajectories for different initial positions projected in the channel cross-section at $Re = 1$ and $\beta = 0.15$: (a) for $Wi = 0.01$, $El = 0.01$, almost all particles migrate towards the channel centreline; (b) for $Wi = 0.1$, $El = 0.1$, the particles released near the wall move towards the corner along the wall; (c) for $Wi = 0.5$, $El = 0.5$, particles migrate faster and the corner attractive region is enlarged as Wi increases; and (d) for $Wi = 1.0$, $El = 1.0$, the corner attractive region shrinks as Wi further increases. Owing to symmetry, only the upper-right quadrant of the channel is considered. The dash-dotted lines delimit the region accessible to the particles. The big dots denote the particle initial positions, and the small dots represent the particle positions on the particle trajectories when the particles travel every 100 dimensionless time units. In (b–d), the red closed lines mark the corner attractive regions.

expected to be very small, and the particle migration is dominated by the fluid inertial effect. It was shown in the experiments of Choi *et al.* (2011) and Abbas *et al.* (2014) that the particles suspended in Newtonian square channel flow at $Re \approx 100$ migrated towards the channel walls along the cross-stream direction at the first stage and then migrated slowly towards the face centres at the second stage, with the migration rate being around one order smaller compared to that at the first stage, and at $Re \approx 10$ the second-stage migration did not occur and only the particle ring (annulus) could be observed. In our simulations for $Re = 10$ and $Wi = 0.01$, the particles migrate along the cross-stream direction to an annulus region located at around $0.28H$ away from the channel centreline (the shaded area in figure 4a) and the second-stage migration is not observed, consistent with the experiments of Choi *et al.* (2011) and Abbas *et al.* (2014). Figure 4(b) shows that the particles migrate towards an equilibrium position

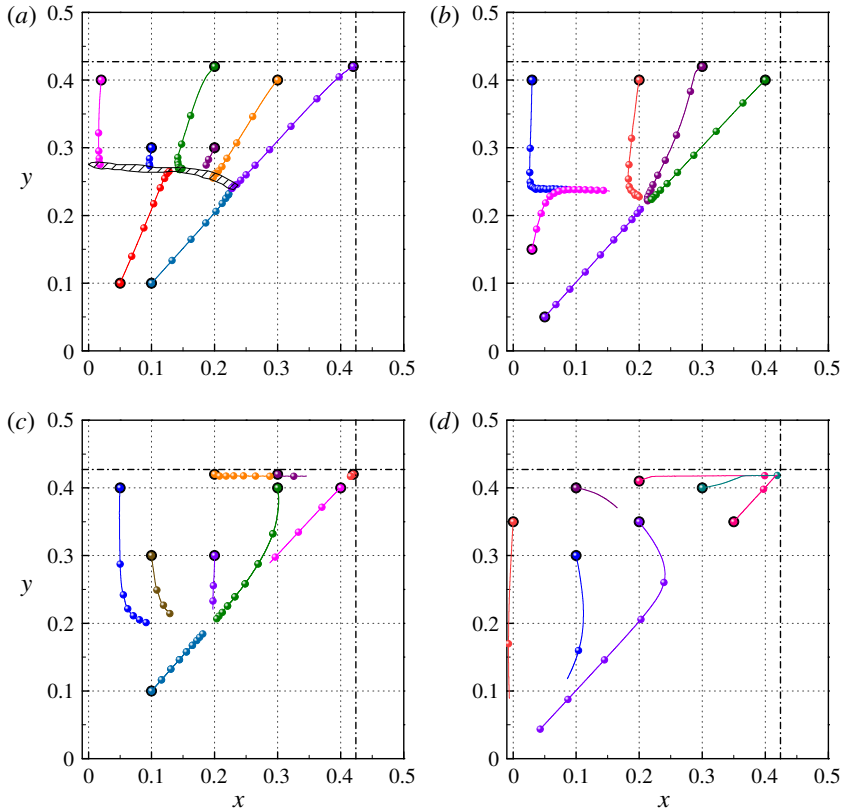


FIGURE 4. (Colour online) Particle trajectories for different initial positions projected in the channel cross-section at $Re = 10$ and $\beta = 0.15$: (a) for $Wi = 0.01$, $El = 0.001$, particles migrate to the shaded ring area; (b) for $Wi = 0.05$, $El = 0.005$, there exists only a diagonal equilibrium position; (c) for $Wi = 0.1$, $El = 0.01$, there exist both the diagonal equilibrium position and the corner equilibrium position with small attractive region; and (d) for $Wi = 0.5$, $El = 0.05$, there exist both the centreline and corner equilibrium positions. The big dots denote the particle initial positions, and the small dots represent the particle positions for every 100 dimensionless time units.

located on the diagonal line of the channel cross-section for $Wi = 0.05$ ($El = 0.005$). For $Wi = 0.1$ ($El = 0.01$), besides the diagonal equilibrium position, which is shifted closer to the channel centreline compared to $Wi = 0.05$, the corner equilibrium position with small attractive region appears and the particles released near the wall move towards the corner along the wall, as shown in figure 4(c). From figure 4(d), the channel centreline equilibrium position appears for $Wi = 0.5$ ($El = 0.05$), with the diagonal-line equilibrium position shifted to the centreline. The presence of both centreline and corner equilibrium positions is a feature of viscoelasticity-dominated migration.

The particle trajectories projected in the channel cross-section at $Re = 50$ and $Wi = 0.01, 0.25, 0.5$ and 1.0 (the elasticity number being $0.0002, 0.005, 0.01$ and 0.02 , respectively) are shown in figure 5. For $Re = 50$ and $Wi = 0.01$ ($El = 0.0002$), the fluid inertia dominates the particle migration, and one can see from figure 5(a) that the particles migrate to the ring and then migrate slowly towards the midline equilibrium position. For $Wi = 0.25$ ($El = 0.005$), only the diagonal equilibrium position exists

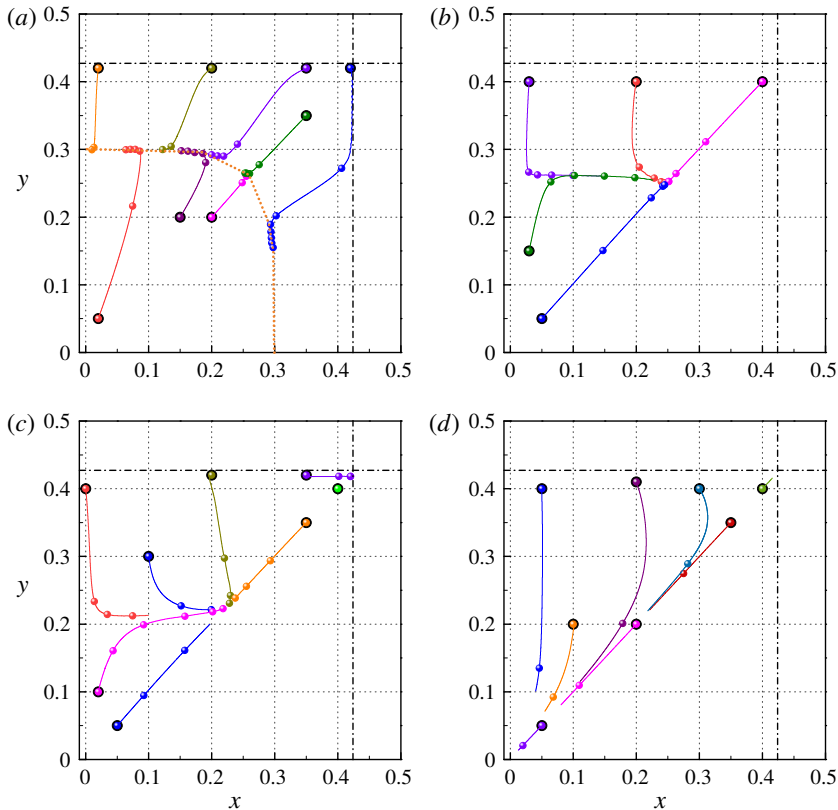


FIGURE 5. (Colour online) Particle trajectories for different initial positions projected in the channel cross-section at $Re = 50$ and $d/H = 0.15$: (a) for $Wi = 0.01$, $El = 0.0002$, particles migrate to the ring marked with the yellow dotted line along the cross-stream direction, and then migrate slowly towards the midline equilibrium position; (b) for $Wi = 0.25$, $El = 0.005$, only the diagonal equilibrium position exists; (c) for $Wi = 0.5$, $El = 0.01$, both diagonal and corner equilibrium positions exist; and (d) for $Wi = 1.0$, $El = 0.02$, both centreline and corner equilibrium positions exist. The big dots denote the particle initial positions, and the small dots represent the particle positions for every 100 dimensionless time units.

(figure 5b). For $Wi = 0.5$ ($El = 0.01$), both diagonal and corner equilibrium positions occur (figure 5c). For $Wi = 1.0$ ($El = 0.02$), both centreline and corner equilibrium positions exist (figure 5d).

The particle trajectories projected in the channel cross-section at $Re = 100$ and $Wi = 0.02, 0.1, 0.5$ and 1.5 (the elasticity number being 0.0002, 0.001, 0.005 and 0.015, respectively) are shown in figure 6. As the fluid elasticity is enhanced, the equilibrium position undergoes the transition from midline (figure 6a), both midline and diagonal line (figure 6b), diagonal line (figure 6), to both centreline and corner (figure 6d).

The comparison between figures 4(a), 5(a) and 6(a) shows that the inertia-induced migration towards the midline equilibrium position becomes faster as the Reynolds number increases. Our results in figures 3, 4(d), 5(d) and 6(d) indicate that the rate of the elasticity-induced migration towards the channel centreline depends much more strongly on the Weissenberg number than on the elasticity number, although the Reynolds number plays a negative role for the elasticity-induced migration.

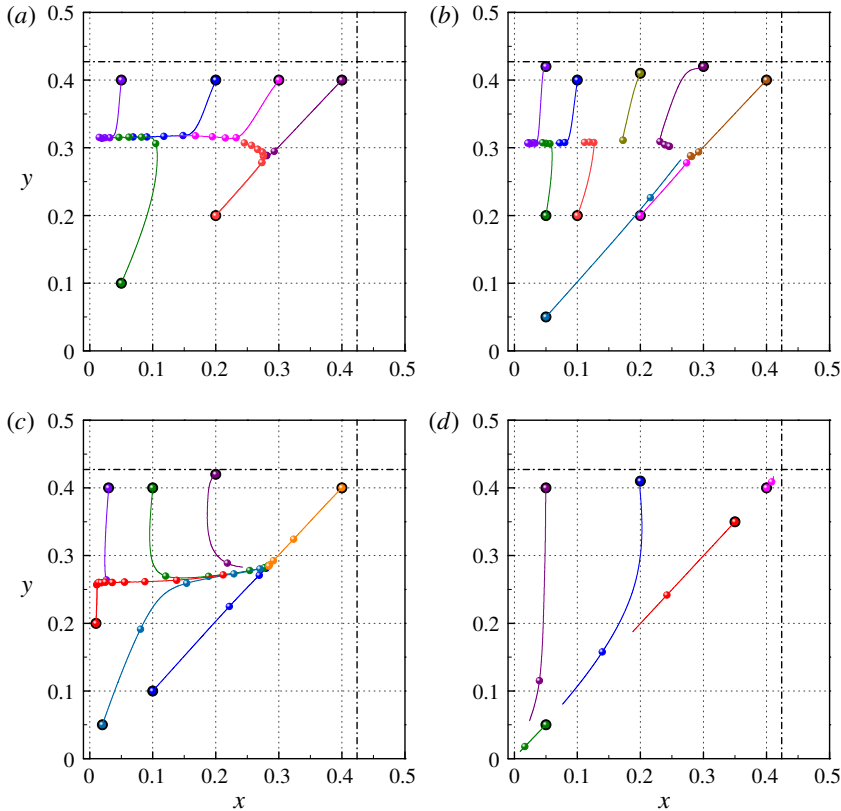


FIGURE 6. (Colour online) Particle trajectories for different initial positions projected in the channel cross-section at $Re = 100$ and $a/H = 0.15$: (a) for $Wi = 0.02$, $El = 0.0002$, particles migrate towards the midline equilibrium position; (b) for $Wi = 0.1$, $El = 0.001$, both the midline and diagonal equilibrium positions exist; (c) for $Wi = 0.5$, $El = 0.005$, only the diagonal equilibrium position exists; and (d) for $Wi = 1.5$, $El = 0.015$, both centreline and corner equilibrium positions exist. The big dots denote the particle initial positions, and the small dots represent the particle positions for every 100 dimensionless time units.

In addition, the corner attractive area for the same Weissenberg number becomes smaller for a higher Reynolds number, as expected.

3.1.3. Phase diagram for the equilibrium positions

We have shown that the midline, diagonal line, corner and centreline equilibrium positions occur successively as the fluid elasticity is enhanced, when the fluid inertia is significant. The diagonal-line EP (abbreviation for ‘equilibrium position’ or ‘equilibrium positions’) can exist alone or coexist with the midline and corner EP. The numerical results of Li *et al.* (2015) showed that the transition between the off-centreline (or midline) and centreline EP depended on both elasticity and Reynolds numbers (but more strongly on the elasticity number than on the Reynolds number) for the particle elasto-inertial migration in the midplane of a square channel. Here, we examine the dependence of our EP on the elasticity and Reynolds numbers, and the phase diagram is plotted in figure 7(a). It can be seen that the equilibrium position depends strongly on the elasticity number and weakly on the Reynolds

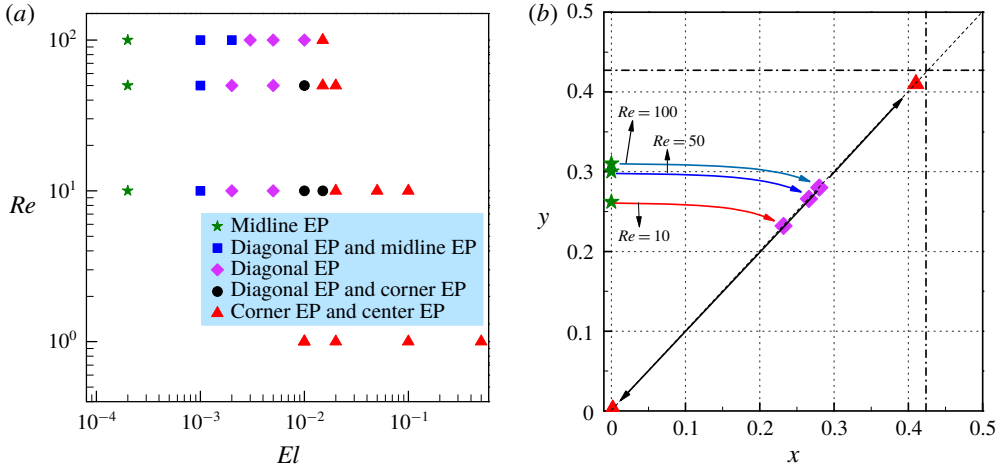


FIGURE 7. (Colour online) (a) Phase diagram for the equilibrium positions as a function of Re and El . ‘EP’ is the abbreviation of ‘equilibrium position’. (b) Schematic diagram for the equilibrium positions changing with Re and El . The arrows guide the transition of the equilibrium position from midline, diagonal line and to centre and corner of the channel cross-section, as El increases.

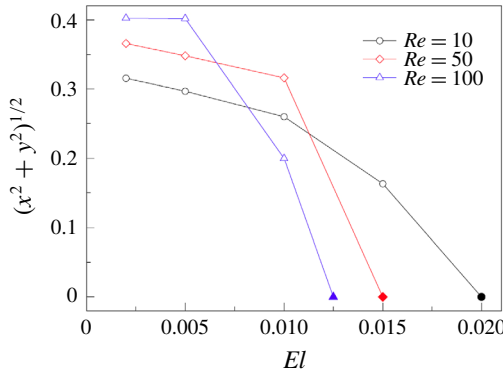


FIGURE 8. (Colour online) The distances away from the channel centreline of the diagonal-line equilibrium positions as a function of El at different Reynolds numbers.

number. For $Re = 10$ – 100 , the diagonal-line EP occurs largely at $El = 0.001$ – 0.15 . For $El = 0.015$, the equilibrium position for $Re = 10$ is located on the diagonal line, whereas those for $Re = 50$ and 100 are located on the channel centreline, indicating that the critical elasticity number for the centreline EP decreases with increasing Reynolds number, in qualitative agreement with the observation of Li *et al.* (2015). A schematic diagram for the equilibrium positions changing with Re and El is presented in figure 7(b). The arrows therein guide the transition of the equilibrium position from midline, diagonal line and to centre and corner of the channel cross-section, as El increases.

The distances away from the channel centreline of the diagonal-line equilibrium positions as a function of El at $Re = 10, 50$ and 100 are plotted in figure 8. The midline EP and the diagonal-line EP at very low elasticity numbers are located farther away from the channel centreline at a larger Reynolds number. However, the diagonal-

line equilibrium positions are shifted towards the channel centreline more rapidly with increasing elasticity number at a larger Reynolds number, leading to a lower critical transition elasticity number for a higher Reynolds number.

Li *et al.* (2015) compared their numerical prediction of the critical transition elasticity number to the theoretical value from the balance between the elastic force and the inertia-induced force. We here conduct similar analysis, following their work. The elastic force derived by Ho & Leal (1976) has the form for two-dimensional Poiseuille flow of an Oldroyd-B fluid (Li *et al.* 2015):

$$F_e = \frac{40}{3} \pi \rho_f U_0^2 d^2 \frac{d}{H} El(1 - \eta_r) y^*, \quad (3.1)$$

where y^* is the dimensionless lateral position in the range of -0.5 to 0.5 . The inertia-induced force derived by Ho & Leal (1974) for the two-dimensional Poiseuille flow at low particle Reynolds numbers is

$$F_i = C(y^*) \rho_f U_0^2 d^2 \left(\frac{d}{H} \right)^2, \quad (3.2)$$

where C is a function of y^* and has the maximum value of around 0.24 at $y^* \approx 0.15$. The balance between the elastic and inertial forces at $y^* = 0.15$ yields the critical elasticity number $El_c \approx 0.038(d/H)(1/(1 - \eta_r))$, which is around 0.011 for $d/H = 0.15$ and $\eta_r = 0.5$, comparable to our prediction for $Re = 100$ in figure 8.

3.1.4. Effects of channel length, blockage ratio and Giesekus model

The diagonal-line EP for a rigid spherical particle in a viscoelastic channel flow has not been reported previously, to the best of our knowledge. The experiments on particle migration in viscoelastic square channel flow were conducted for relatively large elasticity numbers (typically $El > 0.1$). We attempt to examine whether the presence of the diagonal-line EP is dependent on other factors that have not been considered so far, such as the effects of the channel length, the particle size and the fluid rheological property. The channel length of $L = H$ is relatively small, and the hydrodynamic interactions between the particle and its periodic images might be important. In order to examine the effect of the channel length, simulations for $L = 2H$ at $Re = 50$ and $Wi = 0.5$ are performed, and the results on the particle trajectories are shown in figure 9(b). The particle trajectories for $L = H$ at $Re = 50$ and $Wi = 0.5$ are shown in figure 9(a) for comparison. For $L = 2H$, the diagonal-line EP still exists, although its position is shifted a little closer to the channel centreline, compared to the case of $L = H$.

Figure 9(c) shows the particle trajectories for the blockage ratio of 0.1 (the blockage ratio being defined as the ratio of the particle diameter to the channel width, d/H), and the particles migrate towards the diagonal-line EP, which is closer to the centreline compared to the case of $d/H = 0.15$. This is consistent with the theoretical prediction (Ho & Leal 1974, 1976) that the inertial effect decreases more significantly than the elastic effect as the particle size decreases, since the elastic force is proportional to d^3 (equation (3.1)), while the inertial force is proportional to d^4 (equation (3.2)).

The Oldroyd-B model is characterized by a constant viscosity. The Giesekus model is a typical constitutive model for various polymer solutions with the shear-thinning property and a non-zero second normal stress difference, which leads to the secondary flow in a square channel (Villone *et al.* 2013; Li *et al.* 2015). The secondary flow is

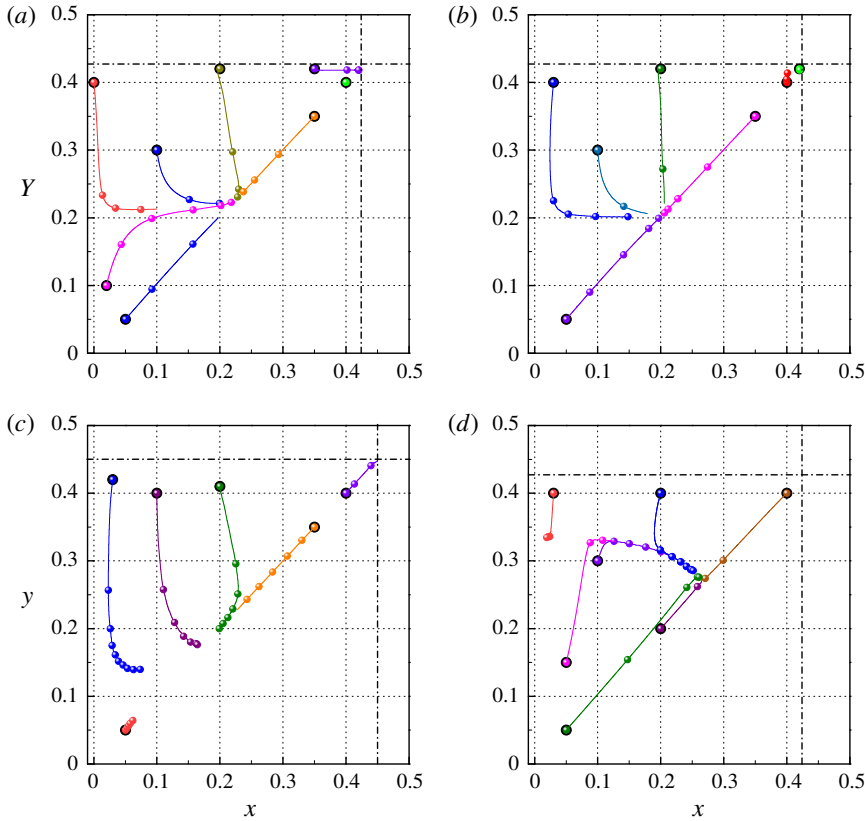


FIGURE 9. (Colour online) Particle trajectories for different initial positions projected in the channel cross-section at $Re=50$ and $Wi=0.5$ (i.e. $El=0.01$): (a) $L=H$, $d/H=0.15$; (b) $L=2H$, $d/H=0.15$; (c) $L=H$, $d/H=0.1$; and (d) $L=H$, $d/H=0.15$ and Giesekus model with $\alpha=0.2$. The big dots denote the particle initial positions, and the small dots represent the particle positions for every 100 dimensionless time units.

characterized by eight circulations in the cross-section with the flow direction pointing to the channel centreline along the diagonal line. The Giesekus constitutive equation can be written as follows:

$$\frac{\partial \mathbf{B}}{\partial t} + \mathbf{u} \cdot \nabla \mathbf{B} - \mathbf{B} \cdot \nabla \mathbf{u} - (\nabla \mathbf{u})^T \cdot \mathbf{B} + \frac{\alpha}{Wi} (\mathbf{B} - \mathbf{I})^2 + \frac{\mathbf{B} - \mathbf{I}}{Wi} = 0 \quad \text{in } \Omega, \quad (3.3)$$

where α is a parameter in the Giesekus model, which reduces to the Oldroyd-B model for $\alpha=0$. The particle trajectories projected in the cross-section of a channel filled with a Giesekus fluid with $\alpha=0.2$ for $L=H$, $d/H=0.15$, $Re=50$ and $Wi=0.5$ are plotted in figure 9(d). The diagonal-line EP can also be observed in the Giesekus fluid, which is located farther away from the channel centreline compared to the Oldroyd-B case. Li *et al.* (2015) also observed that the equilibrium position in the midline for the Giesekus fluid was closer to the wall than that for the Oldroyd-B fluid at the same flow conditions. They attributed the reason to the effects of the shear-thinning and secondary flow. The secondary flow points to the wall on the midline and thus tends to push the particle on the midline towards the wall. By contrast, the secondary flow

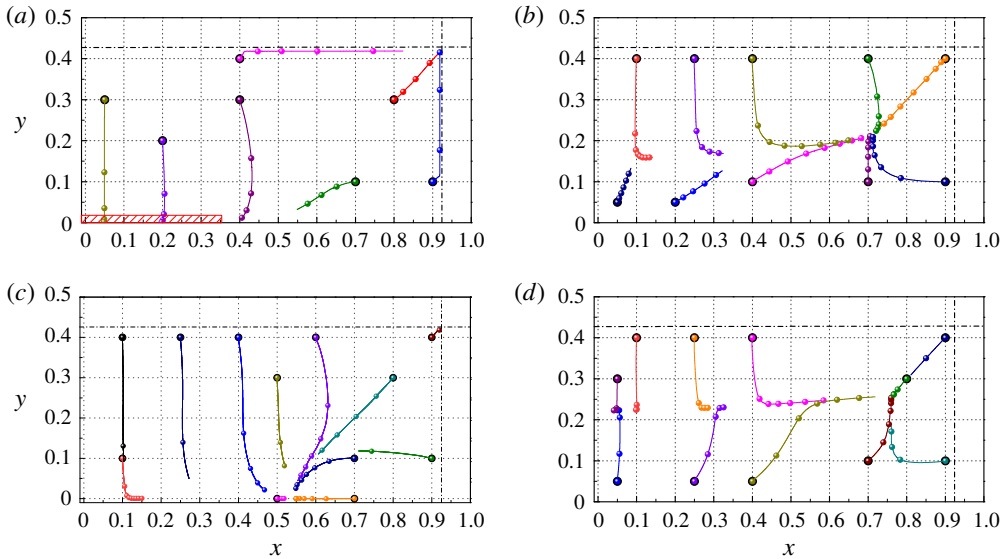


FIGURE 10. (Colour online) Particle trajectories for different initial positions projected in the channel cross-section: (a) at $Re = 1$, $Wi = 0.5$, $El = 0.5$, the fluid viscoelasticity drives particles towards the cross-section corner or shaded area; (b) at $Re = 50$, $Wi = 0.5$, $El = 0.01$, particles migrate towards the diagonal-line EP (equilibrium position); (c) at $Re = 50$, $Wi = 1.0$, $El = 0.02$, an off-centre long-midline EP occurs; and (d) at $Re = 100$, $Wi = 0.5$, $El = 0.005$, particles migrate towards the diagonal-line and short-midline EP. Here $d/H = 0.15$.

points to the channel centreline on the diagonal line and consequently tends to push the particle on the diagonal line towards the centreline. Therefore, the shear-thinning effect should be the primary reason for the equilibrium position being shifted farther away from the channel centreline. In addition, the elastic effect of the Giesekus fluid for the same Reynolds and Weissenberg numbers is weaker than that of the Oldroyd-B fluid, which is expected to be partly responsible for the shift of the equilibrium position observed above. We note that this section (§ 3.1.4) is the only one in the present study to discuss the effect of the Giesekus fluid.

3.2. Particle migration in rectangular channel flow

3.2.1. Elasto-inertial migration equilibrium positions

Our results have revealed a diagonal-line EP for the particle migration in square channel flow. We now further investigate the particle migration in a rectangular channel with an aspect ratio of 2, to see whether similar EP would exist in rectangular channel flow. The results on the particle trajectories for $(Re, Wi, El) = (1, 0.5, 0.5)$, $(50, 0.5, 0.01)$, $(50, 1.0, 0.02)$ and $(100, 0.5, 0.005)$ are shown in figure 10. It is interesting that similar ‘diagonal-line’ EP does occur for the cases of $(Re, Wi, El) = (50, 0.5, 0.01)$ (figure 10b) and $(100, 0.5, 0.005)$ (figure 10d), the same parameters at which the diagonal-line EP occur for the square channel flow (see figures 5c and 6c). For $(Re, Wi, El) = (50, 1.0, 0.02)$, the ‘diagonal-line’ EP disappears in figure 10(c), as the El number is increased to 0.02. The diagonal-line EP is shifted to the channel centreline for the square channel (figure 5d), whereas it is shifted to an off-centre

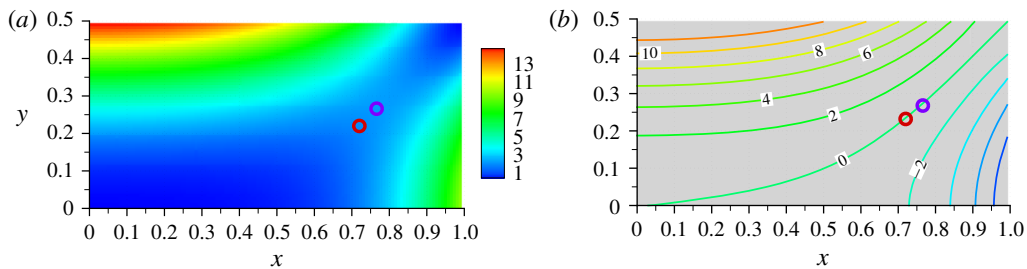


FIGURE 11. (Colour online) (a) Contour map for $(du/dx)^2 + (du/dy)^2$. (b) Contour lines for $(du/dx)^2 - (du/dy)^2$, with values marked on the lines, showing that the particle equilibrium positions are located on the line where $(du/dx)^2 = (du/dy)^2$. The red and violet circles represent the particle equilibrium positions for $(Re, Wi) = (50, 0.5)$ and $(Re, Wi) = (100, 0.5)$, respectively.

position located on the long midline. The channel centreline EP is expected if the elasticity number is further increased above a critical value. Since a relatively large Wi number is limited by our code, the viscoelasticity-dominated particle migration behaviour is examined at a low-Reynolds-number case of $(Re, Wi, El) = (1, 0.5, 0.5)$. The results are shown in figure 10(a), from which the particles released near the wall or the corner migrate towards the corner, and the other particles migrate towards a region on the long midline with the distance away from the centreline being less than roughly $0.35H$. Further migration along the long midline cannot be identified clearly with our code, and it is not clear whether this is a numerical artifact. Migration towards the centreline is expected if the fluid elasticity is further enhanced. In addition, it is shown later that the particle size has significant effects on the particle migration along the long midline at low Reynolds numbers, and smaller particles with $d/H = 0.1$ migrate towards the channel centreline (figure 12a).

For $Wi = 0.5$, as Re is increased from 50 to 100, the ‘diagonal-line’ EP is shifted farther away from the centreline (see figure 10b and 10d), and, on the other hand, an EP on the short midline appears (figure 10d). It is known that, for Newtonian rectangular channel flow, the fluid inertia drives particles to move towards the EP located on the short midline (Zhou & Papautsky 2013), and also the EP on the long midline if Re exceeds a critical value (Liu *et al.* 2015a). Our results indicate that the important elasto-inertia EP for relatively small particles undergoes the transition from midline, ‘diagonal line’, off-centre long midline and channel centreline. The corner EP may appear together with the off-centre long-midline EP and the centreline EP, but is not so important for the non-shear-thinning fluids since its attractive region is always small compared to the area of the channel cross-section.

For the non-square rectangular channel, the ‘diagonal-line’ EP is actually not located on the diagonal line, as shown in figure 10. Considering that the shear of the flow is the driving factor for the particle lateral migration, we conjecture that the ‘diagonal-line’ EP is related to the competition between the shear effects from two lateral directions. Figure 11(b) shows the contours of $(du/dx)^2 - (du/dy)^2$ (here u being the mainstream velocity of the undisturbed channel flow for $Wi = 0.5$) and the particle equilibrium positions for $(Re, Wi) = (50, 0.5)$ and $(100, 0.5)$. One can see that both equilibrium positions are located on the line where the shear rates in two lateral directions are equal to each other, i.e. $(du/dx)^2 = (du/dy)^2$. The contour map for $(du/dx)^2 + (du/dy)^2$ is shown in figure 11(a), which indicates that the

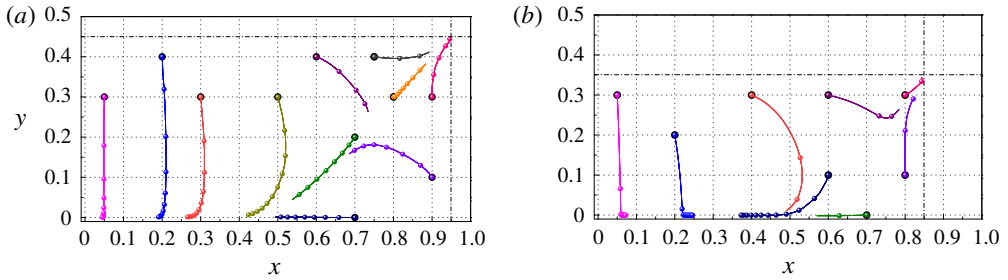


FIGURE 12. (Colour online) Particle trajectories for different initial positions projected in the channel cross-section for (a) $d/H = 0.1$ and (b) $d/H = 0.3$, showing the particle-size-dependent focusing behaviour. Here $Re = 1$, $Wi = 0.5$ and $El = 0.5$.

equilibrium positions are located in the region of low total shear rates. It has been well recognized that the elastic force drives particles from the high-shear-rate region to the low-shear-rate region (Ho & Leal 1976; Leshansky *et al.* 2007; Seo *et al.* 2014; Liu *et al.* 2015b). The inertial force pushes particle away from the channel centreline. The ‘diagonal-line’ EP can be easily understood by considering the combined effects of the elastic and inertial forces.

3.2.2. Particle-size-dependent focusing behaviour

Liu *et al.* (2015b) observed in their experiments that the particles with the blockage ratio of 0.1 in rectangular microchannels with the aspect ratio of 1–4 were focused along the channel centreline, whereas the focusing position of the particles with the blockage of 0.3 was shifted away from the centreline in the direction of the long midline for Reynolds numbers of order 1 and large elasticity numbers. Di *et al.* (2016) and Xiang *et al.* (2016) also observed off-centreline focusing positions in planes parallel to the shorter walls at $Re < 1$. The presence of the off-centreline equilibrium position at low Reynolds numbers is surprising, since the inertial effect that drives particles away from the centreline is expected to be small. Here, simulations are performed for $d/H = 0.1$ and 0.3 at $Re = 1$ and $Wi = 0.5$, in an attempt to check whether the observation of Liu *et al.* (2015b) can be reproduced numerically. The results on the particle trajectories are presented in figure 12. It is interesting that the observation of Liu *et al.* (2015b) is reproduced successfully: the particles with $d/H = 0.1$ migrate towards the channel centreline, while the particles with $d/H = 0.3$ migrate towards an off-centreline EP located in the long midline, as shown in figure 12. Liu *et al.* (2015b) provided an explanation for their observation, which was proposed by Huang *et al.* (1997) to account for the effect of the blockage ratio on the viscoelasticity-induced particle migration in plane Poiseuille flow. The numerical results of Huang *et al.* (1997) indicated that the particle in plane Poiseuille flow with $d/H = 0.025$ migrated all the way towards the channel centre, whereas the particle with $d/H = 0.25$ migrated towards the wall for $Re = 0$ and different Weissenberg numbers. Huang *et al.* (1997) assumed that for a small blockage ratio the migration of the particle is controlled by the normal stresses through the curvature of the velocity profile which push the particle towards the centreline, as predicted by the perturbation solution of Ho & Leal (1976), and in contrast, for a large blockage ratio, the strong effects of the wall blockage overwhelm the effects of the curvature of the velocity profile and increase the effects of the compressive normal stresses

acting on the particle surface so as to drive the particle towards the wall. This mechanism cannot fully explain the off-centre position on the long midline for the three-dimensional rectangular channel flow, because according to this mechanism the particle released near the short midline (the pink trajectory in figure 12*b* for $d/H = 0.3$) should move towards the long wall, instead of moving towards the long midline. Nevertheless, the numerical results of Huang *et al.* (1997) indicated that the elastic effects on the particle migration can be strongly modulated by the blockage ratio, and therefore it is not impossible that the elastic effects drive a large particle in rectangular channel flow with bidirectional shear actions towards an off-centre position on the long midline, rather than on the short midline. The inertial effect could push the particle away from the channel centreline, but the results are similar when we decrease the Reynolds number from 1 to 0.2.

3.2.3. Force analysis

Finally, we attempt to determine which type of force is mainly responsible for the particle migration. For this purpose, we fix the lateral position (x_0, y_0) of a particle which moves in the streamwise direction and rotates freely, and then calculate the different types of forces on the particle. Our fictitious domain method is a non-boundary-fitted method, and thus interpolation is needed to compute the stresses on the particle surface. For a particle with a fixed lateral position $(x_0, y_0) = (0.2, 0)$, the total hydrodynamic force in the x direction, F_x , can be decomposed into the pressure force, F_p , the viscous force, F_V , and the polymer force, F_E , which have the following forms:

$$F_p = \int_{\partial P} -n_x p \, dS, \tag{3.4}$$

$$F_V = \eta_s \int_{\partial P} \left[2n_x \frac{\partial u_x}{\partial x} + n_y \left(\frac{\partial u_x}{\partial y} + \frac{\partial u_y}{\partial x} \right) + n_z \left(\frac{\partial u_x}{\partial z} + \frac{\partial u_z}{\partial x} \right) \right] dS, \tag{3.5}$$

$$F_E = \int_{\partial P} (n_x \tau_{xx} + n_y \tau_{xy} + n_z \tau_{xz}) \, dS. \tag{3.6}$$

The polymer force, F_E , can be further decomposed into the polymer normal force, F_{En} , and the polymer shear force, F_{Es} :

$$F_{En} = \int_{\partial P} n_x \tau_{xx} \, dS, \tag{3.7}$$

$$F_{Es} = \int_{\partial P} (n_y \tau_{xy} + n_z \tau_{xz}) \, dS. \tag{3.8}$$

Note that the pressure force in (3.4) is calculated from the pressure that serves to make the fluid satisfy the incompressibility constraint. For the viscoelastic fluid, the average polymer normal stresses or the polymer isotropic stress $(\tau_{xx} + \tau_{yy} + \tau_{zz})/3$ can also be regarded as ‘pressure’, and the elasticity-induced force is related to the normal stress differences (Ho & Leal 1976). Therefore, we decompose the polymer normal force, F_{En} , into the polymer ‘pressure’ force, F_{Enp} , the force from the first normal stress difference, F_{En1} , and the force from the second normal stress difference, F_{En2} :

$$F_{En} = \underbrace{\int_{\partial P} n_x \frac{(\tau_{xx} + \tau_{yy} + \tau_{zz})}{3} \, dS}_{F_{Enp}} + \underbrace{\int_{\partial P} n_x \frac{(\tau_{xx} - \tau_{zz})}{3} \, dS}_{F_{En1}} + \underbrace{\int_{\partial P} n_x \frac{(\tau_{xx} - \tau_{yy})}{3} \, dS}_{F_{En2}}. \tag{3.9}$$

Case	Total force	F_p	F_V	F_E	F_{Es}	F_{En}	F_{Enp}	F_{En1}	F_{En2}
RecWi05Re1d03Y, $\times 10^{-2}$	-2.3	-3.1	0.85	-0.10	0.0051	-0.11	3.8	-3.7	-0.23
RecWi05Re1d03X, $\times 10^{-3}$	0.43	-0.25	1.15	-0.47	0.77	-1.24	1.15	-2.37	-0.013
SquWi05Re1CS, $\times 10^{-3}$	-2.85	-2.65	-0.22	0.01	0.62	-0.61	5.10	-5.40	-0.30
SquWi15Re100CS, $\times 10^{-2}$	-0.64	-0.67	0.45	-0.43	-0.47	0.044	1.10	-1.03	-0.03
SquWi0Re100CS, $\times 10^{-3}$	5.96	4.12	1.84	0	0	0	0	0	0
SquWi0Re100CL, $\times 10^{-4}$	-7.00	1.36	-8.36	0	0	0	0	0	0
SquWi05Re100CL, $\times 10^{-3}$	1.27	0.006	0.062	1.20	1.88	-0.68	-3.35	1.90	0.77

TABLE 1. Forces on the particle with a fixed lateral position (x_0, y_0) for different cases, normalized by $\eta_0 U_0 H$. Here F_p , F_V , F_E , F_{Es} , F_{En} , F_{Enp} , F_{En1} and F_{En2} represent the pressure force, viscous force, polymer force, polymer shear force, polymer normal force, polymer pressure force, first normal stress difference force and second normal stress difference force defined in (3.4)–(3.9), respectively. RecWi05Re1d03X: rectangular channel, $Wi = 0.5$, $Re = 1$, $d/H = 0.3$ and $(x_0, y_0) = (0, 0.2)$. RecWi05Re1d03Y: rectangular channel, $Wi = 0.5$, $Re = 1$, $d/H = 0.3$ and $(x_0, y_0) = (0.2, 0.0)$. SquWi05Re1CS: square channel, $Wi = 0.5$, $Re = 1$, $d/H = 0.15$ and $(x_0, y_0) = (0.2, 0.0)$. SquWi15Re100CS: square channel, $Wi = 1.5$, $Re = 100$, $d/H = 0.15$ and $(x_0, y_0) = (0.2, 0.0)$. SquWi0Re100CS: square channel, $Wi = 0.0$, $Re = 100$, $d/H = 0.15$ and $(x_0, y_0) = (0.2, 0.0)$. SquWi0Re100CL: square channel, $Wi = 0.0$, $Re = 100$, $d/H = 0.15$ and $(x_0, y_0) = (0.2, 0.31)$. SquWi05Re100CL: square channel, $Wi = 0.5$, $Re = 100$, $d/H = 0.15$ and $(x_0, y_0) = (0.2, 0.28)$.

Our results on the forces on the particle with a fixed lateral position (x_0, y_0) at steady state for some cases are presented in table 1. The forces are normalized by $\eta_0 U_0 H$. Note that for the case of ‘RecWi05Re1d03Y’, where the particle lateral position is fixed at $(0, 0.2)$, the forces in the y direction are calculated with the subscripts x and y exchanged in (3.4)–(3.9). Our results indicate that for the elasticity-induced rapid cross-stream migration (RecWi05Re1d03Y, SquWi05Re1CS and SquWi15Re100CS), the pressure force is the most important driving force for the migration, compared to the viscous force and the polymer force, particularly for the low-Reynolds-number cases (RecWi05Re1d03Y and SquWi05Re1CS). Nevertheless, if one adds the polymer pressure force F_{Enp} to the pressure F_p , then the total pressure force plays a negative role in the particle migration, and the force from the first normal stress difference becomes the driving force for the rapid cross-stream migration, consistent with the theory of Ho & Leal (1976). The second normal stress difference is zero for the pure shear flow of the Oldroyd-B fluid, and thus its contribution to the total force is always small, though it is interesting that its direction is always the same as that of the first normal stress difference force. For the inertia-induced rapid cross-stream migration (SquWi0Re100CS), the pressure is also the most important driving force. For the inertia-induced slow cross-lateral migration to the midline EP (SquWi0Re100CL), the pressure plays a negative role, and the viscous shear force becomes the driving force. For the elasticity-induced slow cross-lateral migration to the diagonal-line EP (SquWi05Re100CL), the pressure is not important and both the first normal stress difference and the polymer shear force are important. For the elasticity-induced anomalous slow off-centre migration in the rectangular channel (RecWi05Re1d03X), both the pressure and the first normal stress difference still tend to drive the particle to move towards the channel centreline, and the shear forces including both the viscous and polymer shear forces become the driving forces for the particle off-centre migration, unlike the elasticity-induced rapid cross-stream migration (RecWi05Re1d03Y).

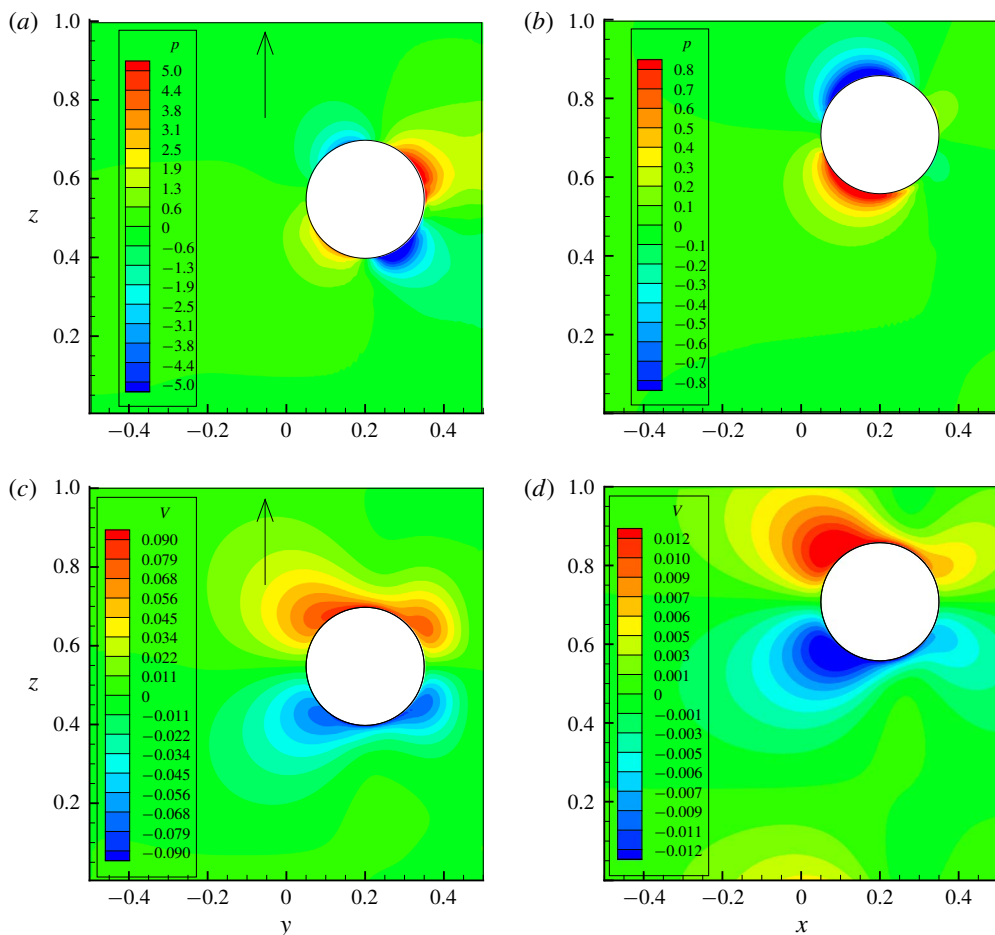


FIGURE 13. (Colour online) Flow fields in the symmetry plane for the particle with a fixed lateral position in a rectangular channel: (a) pressure, $(x_0, y_0) = (0, 0.2)$; (b) pressure, $(x_0, y_0) = (0.2, 0)$; (c) lateral fluid velocity, $(x_0, y_0) = (0, 0.2)$; and (d) lateral fluid velocity, $(x_0, y_0) = (0.2, 0)$. The arrows indicate the flow direction. Here $Re = 1$, $Wi = 0.5$ and $d/H = 0.3$.

The contours of the pressure and the lateral velocity in the symmetry plane for the particles with the fixed lateral positions of $(x_0, y_0) = (0, 0.2)$ (RecWi05Re1d03Y) and $(x_0, y_0) = (0.2, 0)$ (RecWi05Re1d03X) are compared in figure 13. Owing to the significantly different distributions of the shear rate (see figure 11a), there are differences in the distribution pattern of the pressure and the lateral velocity for the two cases. However, it is not clear why the pressure force is important in the inward migration (RecWi05Re1d03Y) and not important in the off-centre migration (RecWi05Re1d03X). We leave the complete understanding of the off-centre EP on the long midline at low Reynolds numbers to a future study.

4. Conclusions

The particle lateral migration in respectively a square channel and a rectangular channel with an aspect ratio of 2, filled with Oldroyd-B fluid, has been simulated numerically with a fictitious domain method. The effects of the fluid inertial and

elastic effects are investigated, in the range of $Re = 1-100$, $Wi = 0.01-1.5$ and $El = 0.0002-1.0$. Throughout this study, the ratio of the solvent viscosity to the total viscosity is $\eta_r=0.5$. The blockage ratio is typically $d/H = 0.15$, and some results for $d/H = 0.1$ and 0.3 have been reported to show the effects of the blockage ratio. From our results, the following conclusions can be drawn.

For particle migration in a square channel:

- (1) When the fluid inertial effect exists, the midline, diagonal-line, corner and channel centreline EP occur successively, as the fluid elastic effects are increased. For $Re = 10-100$, the diagonal-line EP occurs largely at $El = 0.001-0.02$, and can coexist with the midline and corner EP. The transition of the EP depends strongly on the elasticity number and weakly on the Reynolds number. The critical elasticity number for the occurrence of the centreline EP decreases with increasing Reynolds number.
- (2) When the fluid inertia is negligibly small, particles migrate towards the channel centreline, or the closest corner, depending on their initial positions and the Weissenberg number. The corner attractive area first increases and then decreases, as the elasticity number increases.
- (3) The fluid elasticity drives particles to migrate towards the channel centreline along curved lines particularly for $Wi \geq 0.1$ as if they were attracted by the diagonal line, except for the particles released directly on the midline or the diagonal line. The migration rate generally increases with increasing Weissenberg number.

For particle migration in a rectangular channel with aspect ratio of 2:

- (4) The important elasto-inertial migration EP for relatively small particles undergoes the transition from midline, ‘diagonal-line’, off-centre long midline and channel centreline. The ‘diagonal-line’ EP is actually located on the line where two lateral shear rates are equal to each other and the total shear rate reaches its minimum. The ‘diagonal-line’ EP results from the combined effects of the elastic force, which pushes the particle towards a lower-shear-rate region, and the inertial force, which pushes the particle away from the channel centreline.
- (5) The blockage ratio has significant effects on the viscoelasticity-induced particle migration at low Reynolds numbers. The particles migrate towards the channel centreline for $d/H = 0.1$, and towards an off-centre position on the long midline for $d/H = 0.3$ at $Wi = 0.5$ and $Re = 1$. The off-centre migration is driven by the shear forces, unlike the elasticity-induced rapid inward migration, which is driven by the normal force (pressure or first normal stress difference).

Owing to the high computational cost with our code, we have mainly focused on the qualitative understanding of the particle migration in the Oldroyd-B rectangular channel flow, and the quantitative determination of the EP as a function of the parameters is beyond the scope of the present study.

Acknowledgements

The work was supported by the National Natural Science Foundation of China (grant nos 11632016, 11372275).

REFERENCES

- ABBAS, M., MAGAUD, P., GAO, Y. & GEOFFROY, S. 2014 Migration of finite sized particles in a laminar square channel flow from low to high Reynolds numbers. *Phys. Fluids* **26**, 136–157.

- CHOI, Y. S., SEO, K. W. & LEE, S. J. 2011 Lateral and cross-lateral focusing of spherical particles in a square microchannel. *Lab on a Chip* **11**, 460–465.
- CHUN, B. & LADD, A. J. C. 2006 Inertial migration of neutrally buoyant particles in a square duct: an investigation of multiple equilibrium positions. *Phys. Fluids* **18**, 031704.
- D'AVINO, G., GRECO, F. & MAFFETTONE, P. L. 2017 Particle migration due to viscoelasticity of the suspending liquid and its relevance in microfluidic devices. *Annu. Rev. Fluid Mech.* **49**, 341–360.
- D'AVINO, G. & MAFFETTONE, P. L. 2015 Particle dynamics in viscoelastic liquids. *J. Non-Newtonian Fluid Mech.* **215**, 80–104.
- D'AVINO, G., ROMEO, G., VILLONE, M. M., GRECO, F., NETTI, P. A. & MAFFETTONE, P. L. 2012 Single line particle focusing induced by viscoelasticity of the suspending liquid: theory, experiments and simulations to design a micropipe flow-focuser. *Lab on a Chip* **12**, 1638–1645.
- DEL GIUDICE, F., D'AVINO, G., GRECO, F., NETTI, P. A. & MAFFETTONE, P. 2015 Effect of fluid rheology on particle migration in a square-shaped microchannel. *Microfluid. Nanofluid.* **19** (1), 1–10.
- DI, L., LU, X. & XUAN, X. 2016 Viscoelastic separation of particles by size in straight rectangular microchannels: a parametric study for a refined understanding. *Analyt. Chem.* **88**, 12303–12309.
- DI CARLO, D., IRIMIA, D., TOMPKINS, R. G. & TONER, M. 2007 Continuous inertial focusing, ordering, and separation of particles in microchannels. *Proc. Natl Acad. Sci. USA* **104**, 18892–18897.
- GLOWINSKI, R., PAN, T.-W., HESLA, T. I. & JOSEPH, D. D. 1999 A distributed Lagrange multiplier/fictitious domain method for particulate flows. *Intl J. Multiphase Flow* **25**, 755–794.
- HO, B. P. & LEAL, L. G. 1974 Inertial migration of rigid spheres in two-dimensional unidirectional flows. *J. Fluid Mech.* **65**, 365–400.
- HO, B. P. & LEAL, L. G. 1976 Migration of rigid spheres in a two-dimensional unidirectional shear flow of a second-order fluid. *J. Fluid Mech.* **76**, 783–799.
- HU, H. H., PATANKAR, N. A. & ZHU, M. Y. 2001 Direct numerical simulations of fluid–solid systems using the arbitrary Lagrangian–Eulerian technique. *J. Comput. Phys.* **169** (2), 427–462.
- HUANG, P. Y., FENG, J., HU, H. H. & JOSEPH, D. D. 1997 Direct simulation of the motion of solid particles in Couette and Poiseuille flows of viscoelastic fluids. *J. Fluid Mech.* **343**, 73–94.
- KARNIS, A. & MASON, S. G. 1966 Particle motions in sheared suspensions. XIX. Viscoelastic media. *Trans. Soc. Rheol.* **10**, 571–592.
- KAZUMA, M., TOMOAKI, I. & MASAKO, S. S. 2014 Inertial migration of neutrally buoyant spheres in a pressure-driven flow through square channels. *J. Fluid Mech.* **749**, 320–330.
- KIM, B. & KIM, J. M. 2016 Elasto-inertial particle focusing under the viscoelastic flow of DNA solution in a square channel. *Biomicrofluidics* **10**, 024111.
- KIM, J. Y., AHN, S. W., LEE, S. S. & KIM, J. M. 2012 Lateral migration and focusing of colloidal particles and DNA molecules under viscoelastic flow. *Lab on a Chip* **12**, 2807–2814.
- VAN LEER, B. 1979 Towards the ultimate conservative difference scheme. V. A second-order sequel to Godunov's method. *J. Comput. Phys.* **32**, 101–136.
- LESHANSKY, A. M., BRANSKY, A., KORIN, N. & DINNAR, U. 2007 Tunable nonlinear viscoelastic focusing in a microfluidic device. *Phys. Rev. Lett.* **98**, 234501.
- LI, G., MCKINLEY, G. H. & ARDEKANI, A. M. 2015 Dynamics of particle migration in channel flow of viscoelastic fluids. *J. Fluid Mech.* **785**, 486–505.
- LIM, E. J., OBER, T. J., EDD, J. F., DESAI, S. P., NEAL, D., BONG, K. W., DOYLE, P. S., MCKINLEY, G. H. & TONER, M. 2014 Inertio-elastic focusing of bioparticles in microchannels at high throughput. *Nat. Commun.* **5**, 4120.
- LIU, C., HU, G., JIANG, X. & SUN, J. 2015a Inertial focusing of spherical particles in rectangular microchannels over a wide range of Reynolds numbers. *Lab on a Chip* **15**, 1168–1177.
- LIU, C., XUE, C., CHEN, X., SHAN, L., TIAN, Y. & HU, G. 2015b Size-based separation of particles and cells utilizing viscoelastic effects in straight microchannels. *Analyt. Chem.* **87**, 6041–6048.
- LU, X., LIU, C., HU, G. & XUAN, X. 2017 Particle manipulations in non-Newtonian microfluidics: a review. *J. Colloid Interface Sci.* **500**, 182–201.

- MATAS, J. P., MORRIS, J. F. & GUAZZELLI, E. 2004 Inertial migration of rigid spherical particles in Poiseuille flow. *J. Fluid Mech.* **515**, 171–195.
- MATAS, J. P., MORRIS, J. F. & GUAZZELLI, E. 2009 Lateral force on a rigid sphere in large-inertia laminar pipe flow. *J. Fluid Mech.* **621**, 59–67.
- RAFFIIEE, A. H., DABIRI, S. & ARDEKANI, A. M. 2017 Elasto-inertial migration of deformable capsules in a microchannel. *Biomicrofluidics* **11** (6), 064113.
- SEGRE, G. & SILBERBERG, A. 1961 Radial particle displacements in Poiseuille flow of suspensions. *Nature* **189**, 209–210.
- SEO, K. W., KANG, Y. J. & LEE, S. J. 2014 Lateral migration and focusing of microspheres in a microchannel flow of viscoelastic fluids. *Phys. Fluids* **26**, 063301.
- SHAO, X., YU, Z. & SUN, B. 2008 Inertial migration of spherical particles in circular Poiseuille flow at moderately high Reynolds numbers. *Phys. Fluids* **20**, 103307.
- TROFA, M., VOCCIANTE, M., D'AVINO, G., HULSEN, M. A., GRECO, F. & MAFFETTONE, P. L. 2015 Numerical simulations of the competition between the effects of inertia and viscoelasticity on particle migration in Poiseuille flow. *Comput. Fluids* **107**, 214–223.
- VILLONE, M. M., D'AVINO, G., HULSEN, M. A., GRECO, F. & MAFFETTONE, P. L. 2011 Simulations of viscoelasticity-induced focusing of particles in pressure-driven micro-slit flow. *J. Non-Newtonian Fluid Mech.* **166**, 1396–1405.
- VILLONE, M. M., D'AVINO, G., HULSEN, M. A., GRECO, F. & MAFFETTONE, P. L. 2013 Particle motion in square channel flow of a viscoelastic liquid: migration versus secondary flows. *J. Non-Newtonian Fluid Mech.* **195**, 1–8.
- WANG, P., YU, Z. & LIN, J. 2018 Numerical simulations of particle migration in rectangular channel flow of Giesekus viscoelastic fluids. *J. Non-Newtonian Fluid Mech.* **262**, 142–148.
- XIANG, N., DAI, Q. & NI, Z. 2016 Multi-train elasto-inertial particle focusing in straight microfluidic channels. *Appl. Phys. Lett.* **109**, 1–16.
- YANG, S., KIM, J. Y., LEE, S. J., LEE, S. S. & KIM, J. M. 2011 Sheathless elasto-inertial particle focusing and continuous separation in a straight rectangular microchannel. *Lab on a Chip* **11**, 266–273.
- YANG, S., LEE, S. S., AHN, S. W., KANG, K., SHIM, W., LEE, G., HYUN, K. & JU, M. K. 2012 Deformability-selective particle entrainment and separation in a rectangular microchannel using medium viscoelasticity. *Soft Matt.* **8**, 5011–5019.
- YU, Z., PHAN-THIEN, N., FAN, Y. & TANNER, R. I. 2002 Viscoelastic mobility problem of a system of particles. *J. Non-Newtonian Fluid Mech.* **104**, 87–124.
- YU, Z. & SHAO, X. 2007 A direct-forcing fictitious domain method for particulate flows. *J. Comput. Phys.* **227**, 292–314.
- YU, Z. & WACHS, A. 2007 A fictitious domain method for dynamic simulation of particle sedimentation in Bingham fluids. *J. Non-Newtonian Fluid Mech.* **145**, 78–91.
- YU, Z., WACHS, A. & PEYSSON, Y. 2006 Numerical simulation of particle sedimentation in shear-thinning fluids with a fictitious domain method. *J. Non-Newtonian Fluid Mech.* **136**, 126–139.
- YUAN, D., ZHAO, Q., YAN, S., TANG, S.-Y., ALICI, G., ZHANG, J. & LI, W. 2018 Recent progress of particle migration in viscoelastic fluids. *Lab on a Chip* **18** (4), 551–567.
- ZHOU, J. & PAPAUTSKY, I. 2013 Fundamentals of inertial focusing in microchannels. *Lab on a Chip* **13**, 1121–1132.